coatings

MDPI

Article

Calcium Hydroxyapatite Coatings: Low-Temperature Synthesis and Investigation of Antibacterial Properties

Laura Lukaviciute [1], Justina Karciauskaite [1], Inga Grigoraviciute [1], Dovile Vasiliauskiene [2], Denis Sokol [1] and Aivaras Kareiva [1,*]

[1] Institute of Chemistry, Vilnius University, Naugarduko 24, LT-03225 Vilnius, Lithuania; lukaviciute.laura@gmail.com (L.L.); justina.karciauskaite@chgf.stud.vu.lt (J.K.); inga.grigoraviciute@gmail.com (I.G.); denis.sokol@chgf.vu.lt (D.S.)

[2] Department of Chemistry and Bioengineering, Vilnius Gediminas Technical University, Saulėtekio al. 11, LT-10223 Vilnius, Lithuania; dovile.vasiliauskiene@vilniustech.lt

* Correspondence: aivaras.kareiva@chgf.vu.lt

Abstract: In the present work, the low-temperature synthesis of substituted calcium hydroxyapatite ($Ca_{10}(PO_4)_6(OH)_2$, HAP) with copper and zinc ions on titanium substrates was performed. Initially, $CaCO_3$ coatings were synthesised on titanium substrate using the sol-gel method at 550 °C in a CO_2 atmosphere. Crystalline calcium hydroxyapatite was then synthesised from these $CaCO_3$ coatings through the dissolution-precipitation method at low temperature (80 °C). X-ray diffraction (XRD) analysis, FTIR and Raman spectroscopies, and scanning electron microscopy (SEM) were employed to evaluate the phase composition, surface functional groups, crystallinity, and morphology of the coatings. The results showed the formation of hexagonal HAP particles with a size of 20 nm at low temperature, exhibiting high homogeneity in particle size distribution. In the calcium hydroxyapatite, some of the Ca^{2+} ions were replaced by Cu^{2+} ions. Heating the mixture of $Ca(NO_3)_2$ and $Cu(NO_3)_2$ solutions at 550 °C in a CO_2 atmosphere led to the formation of copper hydroxide carbonate (malachite, $Cu_2(OH)_2CO_3$) along with $CaCO_3$. The reaction between the sol-gel precursor obtained and Na_2HPO_4 resulted in the formation of copper-substituted hydroxyapatite (Cu-HAP). Different synthesis methods were tested with Zn^{2+} ions, and on the surface of the coating, $Zn(OH)(NO_3)(H_2O)$, $Zn_3(OH)_4(NO_3)_2$, and unreacted $CaCO_3$ were formed. Antibacterial properties of the coatings were tested using the inhibition zone method. No inhibition zones were observed for HAP. However, in the Cu and Zn containing coatings, inhibition zones were observed in the presence of a colony of *B. subtilis* bacteria. However, no inhibition zones were detected in the presence of *E. coli* bacteria.

Keywords: $Ca_{10}(PO_4)_6(OH)_2$; Cu and Zn containing hydroxyapatite; coatings; sol-gel method; dissolution-precipitation method

Citation: Lukaviciute, L.; Karciauskaite, J.; Grigoraviciute, I.; Vasiliauskiene, D.; Sokol, D.; Kareiva, A. Calcium Hydroxyapatite Coatings: Low-Temperature Synthesis and Investigation of Antibacterial Properties. *Coatings* **2023**, *13*, 1991. https://doi.org/10.3390/coatings13121991

Academic Editors: Egemen Avcu, Mert Guney and Yasemin Yıldıran Avcu

Received: 23 October 2023
Revised: 20 November 2023
Accepted: 20 November 2023
Published: 23 November 2023

1. Introduction

Calcium hydroxyapatite ($Ca_{10}(PO_4)_6(OH)_2$, HAP) constitutes the primary inorganic component of bone tissue and exhibits exemplary biocompatibility [1]. Morphologically, hydroxyapatite particles in bone can manifest in diverse geometries—spherical, plate-like, or needle-like—and typically exhibit dimensions on the order of 40–60 nm in length, 20 nm in width, and 1.5–5 nm in thickness [2,3]. Hydroxyapatite accounts for up to 60% of bone tissue by weight and as much as 97% in tooth enamel [1]. Due to its high surface-area-to-volume ratio, reactivity, and biomimetic properties, nano-HAP serves as an optimal material for orthopaedic implant coatings and bone-substitute fillers [4].

Hydroxyapatite-based implant materials often feature a porous, interlinked architecture that mimics the intracellular matrix, thus facilitating cellular proliferation and tissue regeneration [5,6]. This structural design also enhances osseointegration by establishing a rigid mechanical interface with the surrounding biological tissues, thereby minimising fibrous tissue formation [7,8].

This ionic flexibility is in alignment with the naturally occurring human bone mineral, which comprises non-stoichiometric nanocrystalline apatites. These apatites possess structural imperfections owing to the substitution of calcium, phosphate, and hydroxide ions by a range of ions such as Na, Mg, Zn, Sr, K, F, Cl, Si, and CO_3^{2-} [9–11]. Such adaptability underlines the modifiable bioactive properties of HAP through lattice incorporation of diverse substituents [12,13].

Despite the promise of hydroxyapatite coatings, challenges persist in optimising their synthesis and functional properties. Various substrates such as titanium, quartz, and silicon have been employed for the deposition of HAP coatings via the aqueous sol-gel method, which is contingent upon precise control of temperature, pH, and precursor concentrations [14]. This technique, however, typically necessitates elevated temperatures to facilitate the crystallisation of hydroxyapatite, potentially resulting in heterogeneous coatings with domains of varying grain sizes [14]. Furthermore, synthesis of hydroxyapatite coatings on titanium substrates at elevated temperatures may induce the formation of a TiO_2 phase, thereby compromising adhesion to the substrate [15]. Consequently, there is an ongoing pursuit to develop innovative methodologies for synthesising hydroxyapatite coatings that faithfully replicate the characteristics of natural bone tissue.

The objective of this study is to investigate the potential of substituting Ca^{2+} ions with Zn^{2+} and Cu^{2+} ions in HAP coatings using a low-temperature sol-gel dissolution-precipitation deposition approach. The suggested method is promising for the preparation of Cu-HAP coatings; however, the formation of Zn-HAP did not proceed. It was found that in the Cu and Zn containing coatings, inhibition zones were observed in the presence of a colony of *B. subtilis* bacteria. However, no inhibition zones were detected in the presence of *E. coli* bacteria.

2. Materials and Methods

2.1. Synthesis and Materials

2.1.1. Synthesis of Calcium Carbonate

The synthesis of the HAP porous layers was carried out on Ti (Thermo Scientific, Waltham, MA, USA; 1.0 mm thick, 99.2%; CAS 7440-32-6) wafers, which were laser cut (1 × 1 cm) in the open access mechanics centre. The titanium wafers were mechanically abraded to remove the oxide film formed in the air and surface scratches. The titanium plates were mechanically abraded with sandpaper of different grit sizes (1000–2500 grit). The plates were scrubbed for 1 min on each side. The plates were then chemically treated by soaking for 30 min at 70 °C in a solution of 96% 5 mL H_2SO_4 (Chempur, Karlsruhe, Germany, 99.7%) and 7% 0.35 mL HCl (Chempur, 37%). After soaking, the plates were washed in an ultrasonic bath with distilled water and ethanol for 5 min. The cleaned plates were dried overnight at room temperature. The prepared plates were used for the synthesis of $CaCO_3$ and HAP.

For the preparation of the solution, 11.807 g of $Ca(NO_3)_2{\cdot}4H_2O$ (Alfa Aesar, Ward Hill, MA, USA, 99.6%) was weighed and dissolved in 100 mL of ethanol (Vilniaus degtine, Vilniaus, Lithuania, 99.8%). Concentration was 0.5 mol/l. The solution was subjected to magnetic stirring at a temperature of 30 °C until complete dissolution was confirmed. The submerged plates were then placed in a furnace, manufactured by Nabertherm, New Castle, Germany, for heat treatment. A CO_2-rich environment within the furnace was established by positioning ceramic plates coated with activated carbon adjacent to the submerged plates. The furnace was programmed to elevate its internal temperature from an initial 20 °C to 550 °C at a rate of 3 °C/min. Upon reaching 550 °C, this temperature was maintained for a duration of 5 h. During the reaction, $Ca(NO_3)_2$ was thermally decomposed into CaO, followed by a reaction of the CaO with the CO_2 to form calcite. Before removal from the furnace, the furnace was cooled by lowering the temperature to 20 °C at a rate of 3 °C/min.

2.1.2. Synthesis of Calcium Hydroxyapatite

For the synthesis of HAP, a solution was prepared by weighing 0.14 g of Na_2HPO_4 (Carl Roth, Karlsruhe, Germany, 99%) and 0.6057 g of TRIS ($C_4H_{11}NO_3$) (Carl Roth, 99%) buffer. The weighed materials were dissolved in 100 mL of distilled water. The solution was stirred on a magnetic stirrer until dissolved and maintained at 30 °C. The pH of the solution was alkaline (approximately 9–10). After the dissolution of the materials, the solution was poured onto $CaCO_3$-synthesised plates and soaked for 7 days at 80 °C. After removal from the solution, the samples were washed with distilled water, dried, and used for further analysis. The formation of HAP follows this reaction:

$$10\ CaCO_3 + 6Na_2HPO_4 + 2\ H_2O = Ca_{10}(PO_4)_6(OH)_2 + 8\ NaHCO_3 + 2\ Na_2CO_3 \quad (1)$$

2.1.3. Synthesis of Substituted Calcium Hydroxyapatite

In order to introduce Cu^{2+} ions, a mixture of $Ca(NO_3)_2$ and $Cu(NO_3)_2$ was prepared at a concentration of 0.5 mol/l. 5.9036 g of $Ca(NO_3)_2{\cdot}4H_2O$ and 5.814 g of $Cu(NO_3)_2{\cdot}2.5H_2O$ (Sigma-Aldrich, St. Louis, MO, USA, 99.8%) were weighed. The substances were dissolved in 100 mL of ethanol. After the solution had been prepared, the chemically and mechanically treated titanium plates were dropped into the solution in a porcelain dish to submerge. This was then heated in an oven under a CO_2 atmosphere in a previously mentioned manner. After the heating procedure, the plates were dipped into a solution of 0.14 g Na_2HPO_4 + 0.6057 g TRIS buffer (dissolved in distilled water) and soaked for one week at 80 °C. A similar procedure was repeated for the introduction of Zn^{2+} ions (weighed 7.4365 g $Zn(NO_3)_2{\cdot}6\ H_2O$; Chempur, 99.7%). To successfully alloy Zn^{2+} ions, the synthesis was also carried out by direct dropping of already synthesised HAP onto titanium plates into $Zn(NO_3)_2{\cdot}6H_2O$ solution. In total, 7.4365 g of the material was weighed and dissolved in 100 mL of distilled water. A further modification of the Zn-HAP synthesis was also performed. First, $CaCO_3$ was synthesised according to the methodology described for the synthesis of $CaCO_3$ on Ti substrates, then Ti plates containing the synthesised calcium carbonate were dipped into a solution of 0.14 g Na_2HPO_4 + 0.6057 g TRIS buffer + 7.4365 g $Zn(NO_3)_2{\cdot}6$ H2O, which was prepared by dissolving these materials in distilled water.

2.2. Characterisation

X-ray diffraction measurements were carried out to determine the phase composition of the synthesised products. This method of analysis is used to study the crystalline structure. The measurements were carried out on a Rigaku miniFlex II diffractometer (Applied Rigaku Technologies, Inc., Cedar Park, TX, USA) (Cu-Kα radiation, λ = 0.1542 nm at 30 kV 15 mA). The diffracted X-rays were recorded between 10° and 70° (2θ). A Hitachi TM3000 and a Hitachi SU70 (Tokyo, Japan) scanning electron microscope were used to study the morphology and microstructure of the samples. These microscopes were used for EDX analysis of the samples. Raman spectra were recorded at room temperature using a combined Raman and scanning near-field optical microscope (SNOM) WiTec Alpha 300 R (WiTec, Ulm, Germany) with a 532 nm excitation laser source (power 40.9 mW). Fourier transform infrared (FTIR) spectroscopy measurements were carried out on an FTIR spectrometer (PerkinElmer, Inc., Waltham, MA, USA). Evaluation of the antibacterial properties of synthesised coatings on Ti substrates revealed no zones of hydroxyapatite (HAP) inhibition in the presence of Gram-negative Escherichia coli and Gram-positive Bacillus subtilis bacteria. The cultures of *E. coli* and *B. subtilis* bacteria were incubated overnight in liquid LB medium, 10 g/L NaCl, 5 g/L yeast extract, at 37 ° C temperature. After this the culture of bacteria were centrifuged and diluted in sterile 0.9% NaCl to 10^6 units/mL. 100 µL of pre-pared bacteria culture were inoculated in LB agar medium. Plates with HAP, Cu-HAP, and $Zn_3(OH)_4(NO_3)_2$ were placed on these *E. coli* and *B. subtilis* inoculants; prepared samples were incubated at 37 °C temperature for 24 h. After these hours emerges zone of inhibition of HAP, Cu-HAP, and $Zn_3(OH)_4(NO_3)_2$ coatings.

Two or three measurements were conducted in all of the sample preparation and any data processing steps.

3. Results

3.1. Synthesis and Characterization of HAP

The phase composition of the coatings was determined by XRD. The XRD patterns showed that a layer of $CaCO_3$ [PDF:96-154-7348] was formed on the Ti substrate. At 2θ = 29.4°, the most intense peak characteristic of calcite ($CaCO_3$) was visible. The data were in a good agreement with literature [16]. Crystalline calcium hydroxyapatite was then synthesised from these $CaCO_3$ coatings through the dissolution-precipitation method at low temperature (80 °C). The XRD results clearly showed the formation of HAP [PDF: 96-431-7044] with characteristic reflections in the 31–32.5° 2θ angle range (Figure 1). The peaks of $CaCO_3$ [PDF: 96-154-7348] are also identified, proving that some $CaCO_3$ still remains unreacted. In addition, intense diffraction peaks of the Ti substrate are visible. Thus, it can be concluded that a layer of calcium hydroxyapatite has formed on the titanium substrate, which is supported by the literature data [17]. The Raman absorption bands (1084 cm-1, symmetric stretching), (716 cm-1, in-plane bending), (276 and 146 cm- 1, lattice modes) of $CaCO_3$ coating are consistent with calcite [18]. Figure 1 also shows Raman spectrum of HAP coating. The PO_4^{3-} peaks at 590, 950, and 1085 cm^{-1} of the phosphate group oscillations belonging to HAP. The peak around 285 cm^{-1} is attributed to Ca-PO_4 and Ca-OH bonds. The FTIR spectrum of the calcium hydroxyapatite layer on a Ti substrate is depicted in Figure 1 as well. The FTIR spectra shown here identify absorption peaks for PO_4^{3-} (560–600 cm^{-1}, ~600 cm^{-1} and 1000–1100 cm^{-1}), OH^- (3600–3500 cm^{-1} and 630 cm^{-1}), CO_3^{2-} (1460–1530 cm^{-1}), as well as for HPO_4^{2-} (610–615 cm^{-1}) [19]. Thus, it can be concluded that the Raman and FTIR spectroscopy results obtained confirmed the X-ray diffraction data for the successful formation of $Ca_{10}(PO_4)_6(OH)_2$ coatings on the Ti substrate.

The morphological features of the $CaCO_3$ and $Ca_{10}(PO_4)_6(OH)_2$ coatings were investigated by SEM. The calcium carbonate layers were composed of sub-micrometre (up to 1 μm) rhombohedral particles which form a continuous calcite layer. Hexagonal HAP particles of 20 nm in size were formed at low temperature. A particular morphological feature of the synthesised HAP (Figure 1) is that a very high degree of homogeneity and distribution of particle size is achieved.

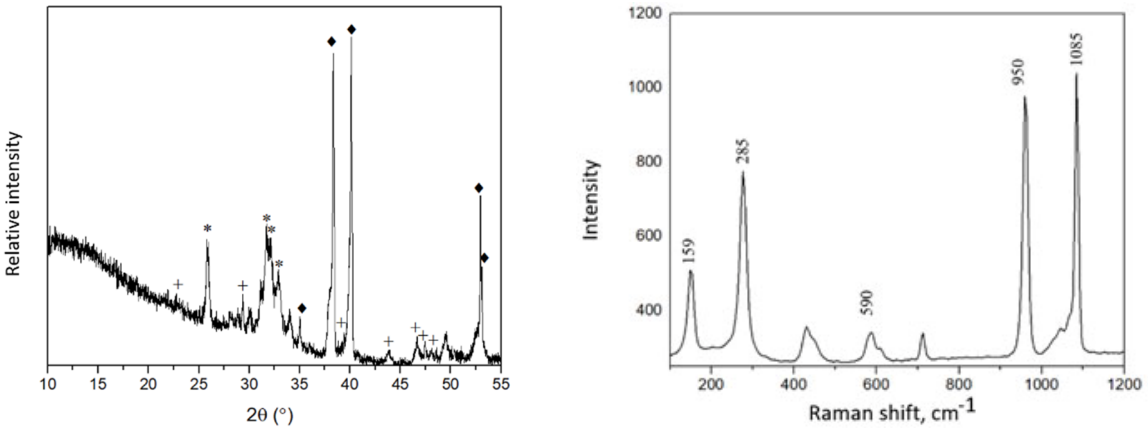

Figure 1. *Cont.*

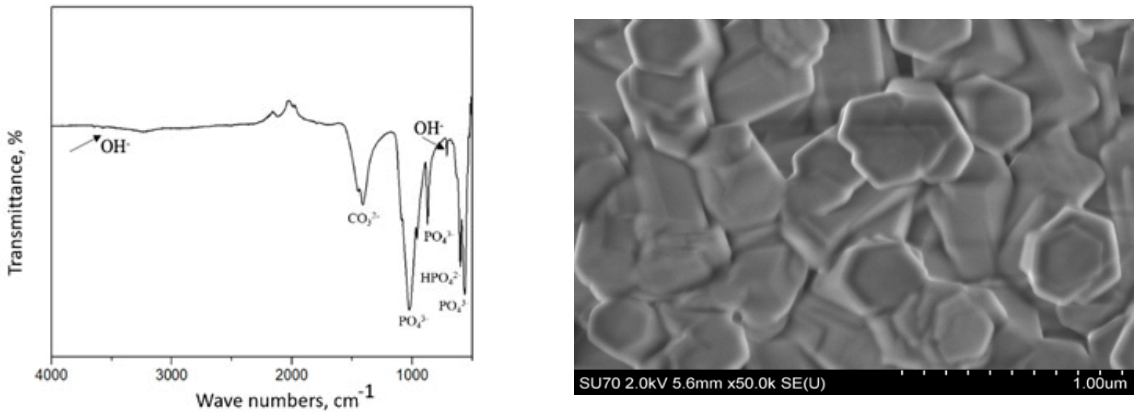

Figure 1. XRD pattern (**top**, **left**), Raman spectrum (**top**, **right**), FTIR spectrum (**bottom**, **left**), and SEM micrograph (**bottom**, **right**) of a calcium hydroxyapatite coating on a Ti substrate. Diffraction reflections: *—HAP [PDF: 96-431-7044]; ♦—Ti [PDF: 96-901-6191]; +—$CaCO_3$ [PDF: 96-154-7348].

3.2. Synthesis and Characterization of Cu-HAP

The phase crystallinity and purity of Cu^{2+}-substituted HAP specimens synthesised by low-temperature sol-gel and dissolution-precipitation method were also investigated by means of XRD analysis. It was determined that during the heating of mixture of $Ca(NO_3)_2$ and $Cu(NO_3)_2$ solutions in a CO_2 atmosphere, in addition to $CaCO_3$, a copper hydroxide carbonate $Cu_2(OH)_2CO_3$ (malachite) had also formed. It is not surprising, since it is known that pure $CuCO_3$ does not form in an aqueous media under normal conditions:

$$2\ Cu(NO_3)_2 + CO_2 + 4\ NaOH \rightarrow Cu_2(OH)_2CO_3 + 4\ NaNO_3 + H_2O \quad (2)$$

Figure 2 represents the XRD patterns of the HAP coatings where Ca^{2+} ions are substituted by Cu^{2+} ions.

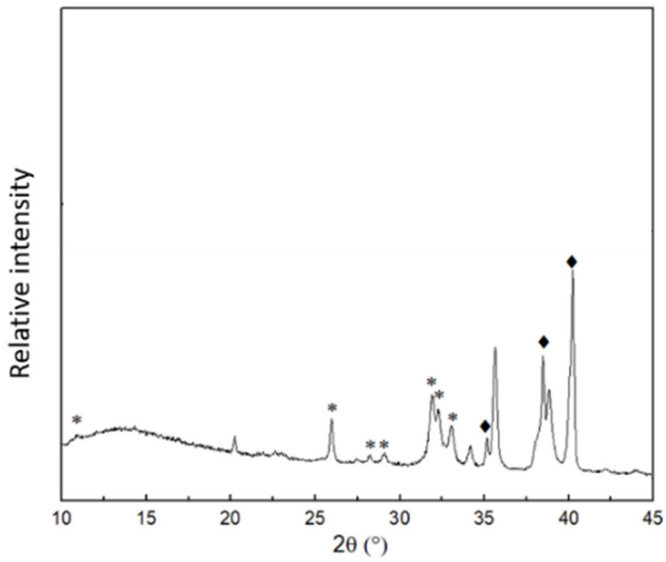

Figure 2. XRD pattern of the Cu-HAP coating obtained on the Ti substrate. Diffraction reflections: *—HAP [PDF: 96-431-7044]; ♦—Ti [PDF:96-901-6191.

The XRD results indicate that the low-temperature precipitation-dissolution method can be successfully used for the synthesis of partially Cu^{2+} ion-substituted HAP. Treatment

of $CaCO_3$ containing a small amount of impure $Cu_2(OH)_2CO_3$ with sodium hydrogen phosphate produces copper-substituted hydroxyapatite (Cu-HAP):

$$10-x\ CaCO_3 + x\ Cu_2(OH)_2CO_3 + 6\ Na_2HPO_4 + 2\ H_2O = Ca_{10-x}Cu_x(PO_4)_6(OH)_2 + x\ Cu(OH)_2 + 8\ NaHCO_3 + 2\ Na_2CO_3 \quad (3)$$

Figure 3 shows the FTIR spectrum of the Cu-HAP coating. The absorption bands at 970 and 1031 cm^{-1} correspond to symmetric and asymmetric vibrations in the PO_4^{3-} ion. Bending vibrations in the PO_4^{3-} ion correspond to absorption bands at 599-567 cm^{-1}. The absorption bands of carbonate are at 870 and 1400 cm^{-1} [20].

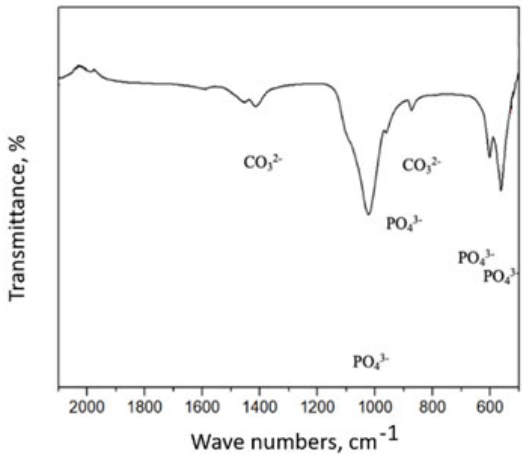

Figure 3. FTIR spectrum of the Cu-HAP coating obtained on the Ti substrate.

Figure 4 represents the Raman spectrum of a HAP coating substituted with Cu^{2+} ions. In this Raman spectrum, the band at 428 cm^{-1} of the phosphate group vibrations are visible, while the bands at 590, 607 cm^{-1} also belong to the PO_4^{3-} asymmetric vibrations of the HAP. The band at 957 cm^{-1} corresponds to a fully symmetric stretching of PO_4^{3-}. The sharpness of this band confirms a good crystallinity of the Cu-HAP coating [21].

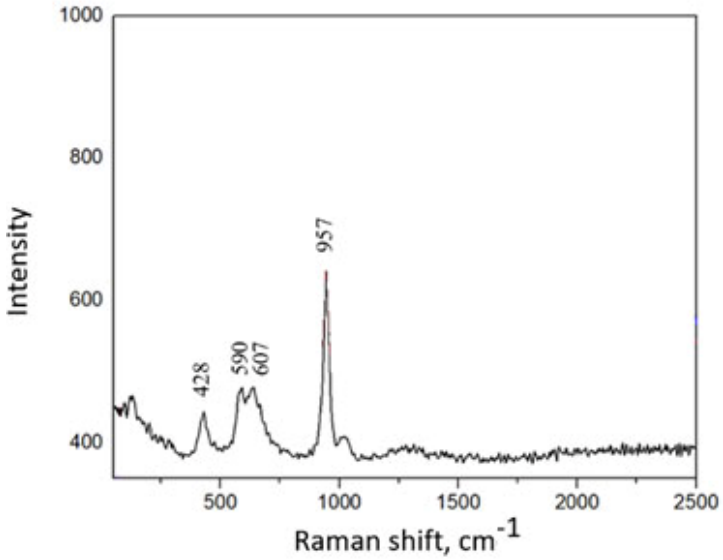

Figure 4. Raman spectrum of the Cu-HAP coating obtained on the Ti substrate.

3.3. Synthesis and Characterization of Zn-HAP

However, the formation of HAP coatings substituted with Zn^{2+} ions by the above preparation method did not proceed. The results presented in the XRD pattern of the coating synthesised by the low-temperature precipitation-dissolution method (by forming

mixed carbonates from a mixture of $Zn(NO_3)_2 \cdot 6H_2O$ and $Ca(NO_3)_2 \cdot 4H_2O$ and dropping the product into Na_2HPO_4 + TRIS buffer solution) confirmed only formation of calcite which was not transformed to the Zn-HAP. Once again, we can conclude that HAP substituted by zinc ions has not formed by this synthesis method. The XRD patterns contained only diffraction reflections of calcium carbonate.

Therefore, different variations of the proposed synthesis method were tested to obtain a Zn-HAP coating on Ti substrate. An attempt was made to synthesise the Zn-HAP coating by direct immersing of the already synthesised HAP coating on Ti into $Zn(NO_3)_2$ solution. The reaction was carried out under the same conditions at 80 °C for one week. The XRD pattern of the resulting product is shown in Figure 5.

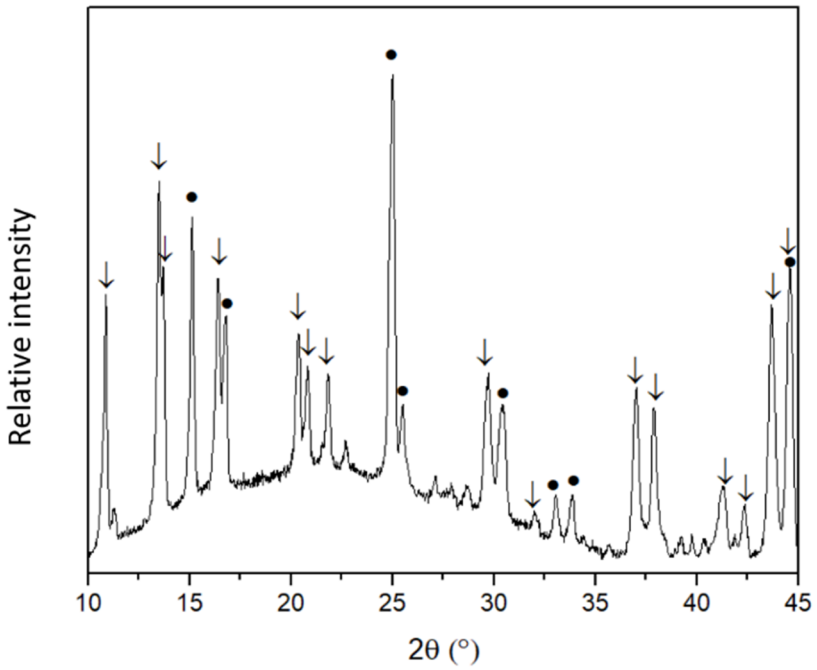

Figure 5. XRD pattern of HAP doped with Zn^{2+} coatings synthesised by immersing the HAP coating on Ti in zinc nitrate solution. Diffraction reflections: •—TiO_2 [PDF: 96-152-8779]; ↓—$Zn(OH)(NO_3)(H_2O)$ [PDF:96-152-9913].

Unexpectedly, the Zn-HAP did not form, and also the HAP coating dissolved, although the solubility of HAP is very low. An even more unexpected result was the formation of almost single phase zinc hydroxide nitrate monohydrate $Zn(OH)(NO_3)(H_2O)$ on the Ti substrate. Thus, during this synthetic approach almost monophasic $Zn(OH)(NO_3)(H_2O)$ instead of Zn-HAP has formed on Ti substrate.

A third synthetic approach was also selected to obtain the Zn-HAP coating. The $CaCO_3$ coating synthesised on Ti substrate was dipped into a solution of Na_2HPO_4 + TRIS buffer + $Zn(NO_3)_2 \cdot 6H_2O$ and stored therein for one week at 80 °C. Again, instead of Zn-HAP, the formation of $Zn(OH)(NO_3)(H_2O)$ along with small amount of $Zn_3(OH)_4(NO_3)_2$ and unreacted calcium carbonate was observed on the Ti surface.

3.4. SEM and EDX Analysis

The SEM images clearly showed that the addition of copper to the HAP also changes the morphology of the particles. Instead of the hexagonal 20 nm particles of HAP, fibrous crystallites with a snowflake shape of about 1 μm have formed (see Figure 6). The volumetric snowflake crystallites are composed of interlocking needles between 0.5 nm and 1 nm in size. Both the partially altered Cu-HAP samples are characterised by a high degree of homogeneity in particle size distribution. The morphology of the Zn^{2+}-containing samples synthesised by forming mixed carbonates from a mixture of $Zn(NO_3)_2 \cdot 6H_2O$ and $Ca(NO_3)_2 \cdot 4H_2O$ and immersing the product into a Na_2HPO_4 + TRIS buffer solution

differs considerably from that of the HAP and Cu-HAP. The representative SEM image of this sample is also shown in Figure 6. It can be seen that homogeneous coatings with some cracks have formed. The coatings are composed of planar crystals larger than 1 μm forming a continuous coating. Few accumulations of smaller particles are also visible on the Ti surface.

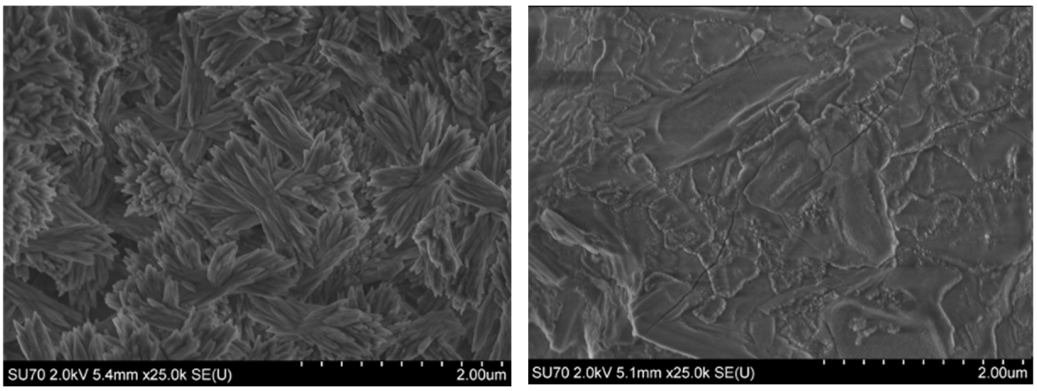

Figure 6. SEM micrographs of Cu-HAP (**left**) of $Zn_3(OH)_4(NO_3)_2$ coatings (**right**) fabricated on Ti substrate.

Elemental analysis of the synthesised Cu and Zn containing coatings was carried out using EDX analysis. The EDX spectra of both samples are presented in Figure 7.

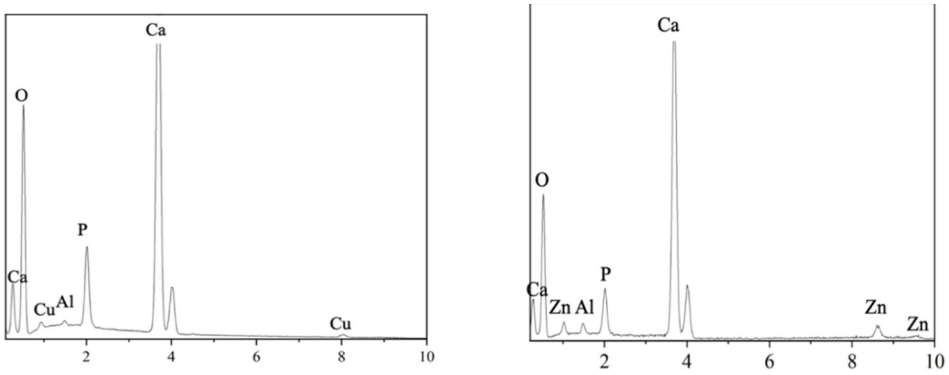

Figure 7. EDX spectra of Cu-HAP (**left**) of $Zn_3(OH)_4(NO_3)_2$ coatings (**right**) fabricated on Ti substrate.

In the case of Cu-HAP coating, the Ca/P ratio of ~1,62 was found to be almost identical to the calcium/phosphorus ratio in stoichiometric HAP (1,67). The molar ratio of calcium to copper was Ca:Cu = 1:0.033, i.e., about 3.3 mol% of the calcium was likely replaced by copper. The formula for the synthesis product could then be written $Ca_{9,7}Cu_{0,3}(PO_4)_6(OH)_2$ or $Ca_{9,85}Cu_{0,15}(PO_4)_6(OH)_2$, if the reaction (see Equation (3)) produced a further stoichiometric amount of copper hydroxide. From the EDX measurements of the sample with zinc, the Ca/P ratio determined was completely unreasonable as it did not correspond to any possible calcium/phosphorus ratio in known phosphates. Although calcium and phosphorus were detected in the synthesised coating, XRD analysis failed to detect calcium phosphate crystalline phases. It is likely that a significant amount of amorphous calcium carbonate and/or a very small amount of calcium hydroxyapatite remained in the coating. The EDX spectrum shows that the coating synthesised contains a significant amount of zinc.

3.5. Antibacterial Properties

Evaluation of the antibacterial properties of synthesised coatings on Ti substrates revealed no zones of hydroxyapatite (HAP) inhibition in the presence of Gram-negative *Escherichia coli* and Gram-positive *Bacillus subtilis* bacteria (Figure 8).

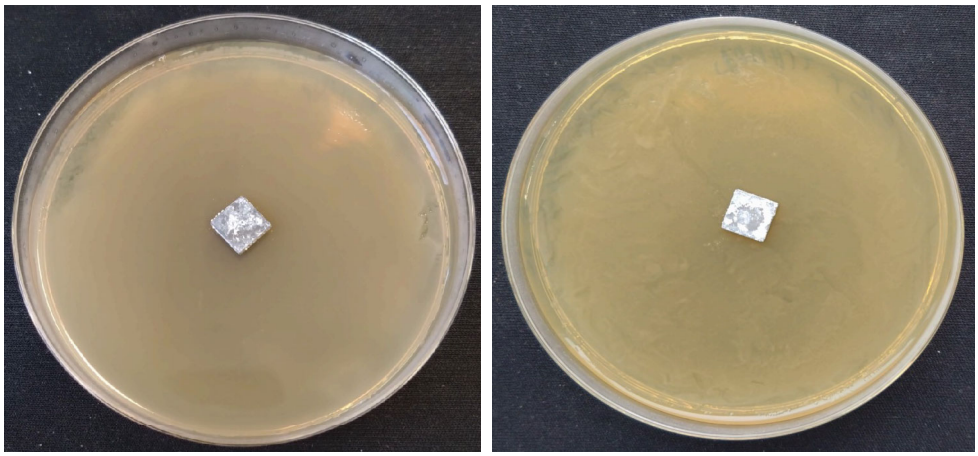

Figure 8. Results of antibacterial performance tests of low-temperature synthesised HAP coatings on Ti with (**left**) *B. subtilis* and (**right**) *E. coli* bacteria.

Subsequent microbiological tests conducted after 24 h of incubation at 37 °C demonstrated zones of inhibition in samples containing Cu-HAP when exposed to a colony of *B. subtilis* (see Figure 9).

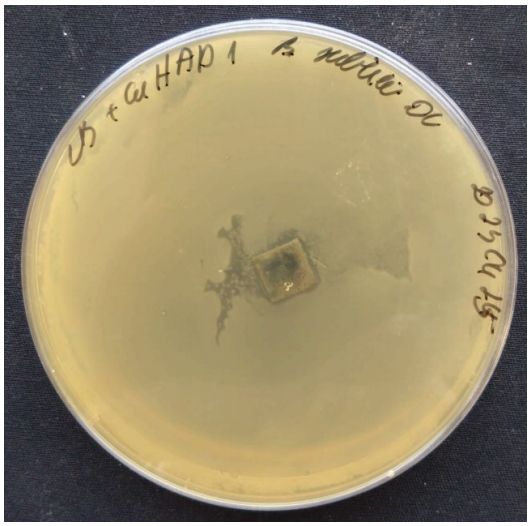

Figure 9. Results of antibacterial performance tests of low-temperature synthesised Cu-HAP coating on Ti with *B. subtilis*.

According to existing literature [22], Gram-positive bacteria possess a negatively charged cell surface and a substantial peptidoglycan membrane, ranging from 20 to 80 nm in thickness. In contrast, Cu^{2+} ions are positively charged and adhere to these negatively charged surfaces, thereby inducing apoptosis in Gram-positive bacteria. Similar observations on the effects of Cu-doped titanium alloy coatings on Gram-positive bacteria have been reported in a study by Kalaivani, S. et al. [23]. Figure 10 illustrates the zones of inhibition associated with samples doped with Zn^{2+} ions when exposed to a *B. subtilis* colony. However, no zones of inhibition were observed in the presence of *E. coli*.

Inhibition zone of coating with Cu-HAP coating on Ti were 10.5mm ± 0.5 mm average from nine measurement; the plate with the $Zn_3(OH)_4(NO_3)_2$ coatings were 15 mm ± 1.8 mm. Several factors may explain the lack of inhibition zones in some cases with Cu^{2+} and Zn^{2+} ion coatings. One plausible explanation is that materials from coatings do not substantially diffuse into the medium; the fraction that does diffuse exhibits inhibitory effects solely against B. subtilis. Another possibility is the absence of direct contact between the metal

ions and the bacteria. Alternatively, the concentrations of metal ions may be insufficient for inhibition.

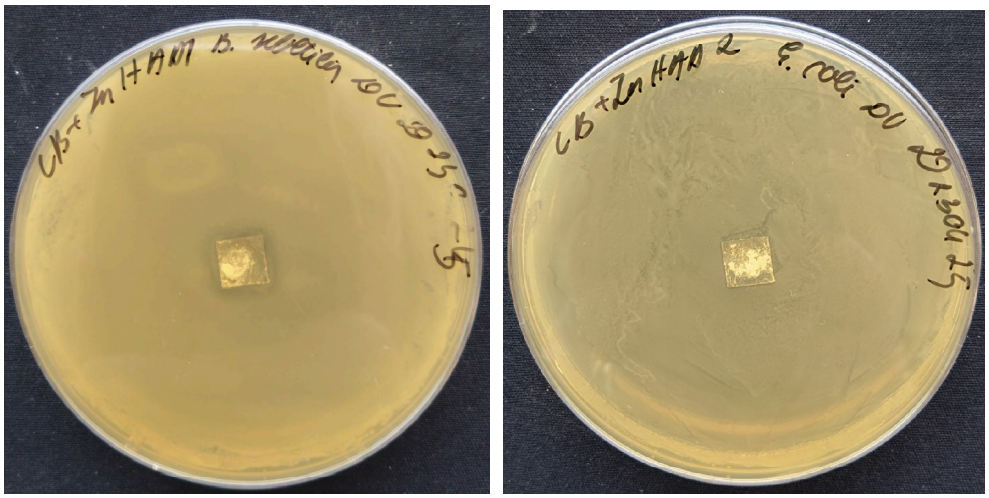

Figure 10. Results of antibacterial performance tests of low-temperature synthesised coatings with Zn^{2+} ions on Ti with (**left**) *B. subtilis* and (**right**) *E. coli* bacteria.

4. Discussion

Bone is a biologically rigid and strong material that lasts for more than 50 years without damage in human bodies [24]. However, an array of factors, including mechanical trauma, age-related weakening, and pathological conditions, necessitate the implantation of synthetic prostheses. [25]. There are different types of bone implants that can be used to help restore or replace bone tissue. The most common are:

1. Metal implants. These implants are usually made of titanium or stainless steel and are used for fracture fixation, joint replacement, and spinal surgery [26].
2. Ceramic implants. These implants are usually made of zirconium and are used for joint replacement surgery [27].
3. Polymer implants. These implants are routinely made of polyethylene and are used for joint replacement surgery, particularly in hips and knees [28].
4. Bone grafts. Bone tissue is taken from another part of the patient's body or from a donor and is used to promote healing of damaged or missing bone [29].

Titanium and calcium phosphate ceramics have emerged as the gold standard in orthopaedic applications. Titanium alloys exhibit commendable mechanical strength and resistance to physiological corrosion, courtesy of an intrinsic oxide layer. Calcium phosphates, particularly hydroxyapatite (HAP), offer unparalleled biocompatibility, accelerating biological responses and promoting strong bone-implant interfaces. Despite their advantages, calcium phosphates are mechanically inferior, leading to research efforts focused on material modification for enhanced bioavailability [25]. HAP has strong osteopermeability properties, making it particularly attractive for biomedical applications [30]. When HAP-based ceramics are implanted, a fibrous layer is formed on the surface of the ceramics, which helps the implant to bond to the living bone. This stabilises the implant and anchors it to the surrounding tissue. Synthetic HAPs are also used to cover metal implants or bone grafts. In addition, a PhD thesis [13] suggests that HAP particles can inhibit the growth of various types of cancer cells. HAP-based materials find utilisation in medical and dental fields as bone graft substitutes, dental implant coatings, and even as facial fillers [31–33].

Various synthesis methodologies have been explored, including wet, dry, and high-temperature techniques, sometimes leveraging bio-waste as precursors, which offers an economical and sustainable approach [34]. Bio-wastes include vertebrate bones, eggshells, and marine shells, the use of which is not only cost-effective but also contributes to sustainability and adds value. The properties of the final product produced depend on the type of

precursor used and the synthesis protocols used. Wet methods are further subdivided into precipitation, sol-gel, hydrothermal, microwave, and sonochemical methods. The precipitation method remains the prevalent approach for synthesising hydroxyapatite (HAP). This technique involves the incremental addition of precursors under constant mixing, while maintaining an alkaline pH. Subsequent to reaction completion, the precipitate is isolated via centrifugation, oven-dried, and mechanically processed. Key variables influencing the material's characteristics include the Ca/P ratio, rate of precursor addition, reaction temperature, and pH, as well as any added dispersants [35]. Advantages of this methodology encompass simplicity, low-temperature synthesis, cost-effectiveness, and high product purity. Limitations include particle non-uniformity and agglomeration, which can be mitigated through meticulous control of reaction parameters [36]. The sol-gel synthesis method is a method for the synthesis of HAP under mild conditions. When the crystallisation of the calcium and phosphate precursors takes place in a mild environment, the resulting HAP has high purity. The rate of gel formation and HAP growth depends on the type of solvent, the precursors used, the pH, and the temperature used in the process. Inaccuracies in these parameters lead to the formation of calcium-containing impurities during the process [37]. Another disadvantage of the sol-gel method is that it is time consuming.

Another widely used method for the preparation of HAP is the hydrothermal method, which involves chemical reactions between calcium and phosphate precursors at temperatures and pressures above ambient conditions. This method produces HAP with high crystallinity and stoichiometry. The morphology, crystallinity, and porosity of the HAP can be controlled by proper control of the pressure and temperature of the reaction vessel [37]. In the microwave (MW) irradiation method, a rapid heating source is used and monodisperse HAP nanoparticles can be synthesised in a short time. In addition, MW methods are energy efficient, the results are reproducible, and the final product has high crystallinity. The method can also be integrated with traditional methods (such as MW-deposition, MW-sol-gel, MW-hydrothermal, etc.) [38]. Research has shown that MW heating can enhance the antibacterial properties of HAP [39]. The sonochemical method is very fast and energy efficient, using ultrasound to synthesise HAP. It has been shown that prolonging the duration of the ultrasound produces small rod-shaped HAP nanoparticles of almost uniform size [40]. Naturally occurring biological resources like animal bones, eggshells, and plant extracts serve as viable precursors for hydroxyapatite (HAP) synthesis. These resources offer cost-effectiveness and waste treatment benefits, alongside yielding biomimetic, biocompatible, and bioactive HAP that is non-stoichiometric due to trace elements, making it analogous to human bone composition [36,41]. Mammalian bones, such as those from cows and pigs, are particularly favoured for their physicochemical resemblance to human bone. The extraction process involves a pre-processing step of cleaning and boiling, followed by high-temperature burning to remove organic compounds [42]. The resultant HAP's properties are influenced by the heating parameters [43–45]. Eggshells, predominantly composed of calcium carbonate, undergo cleaning and heating to form CaO, which is then converted to $Ca(OH)_2$. This is mixed with a phosphorus precursor to synthesise HAP [46]. Plant-derived biomolecules like pectin can modulate HAP morphology. For example, pectin from banana bark has been demonstrated to produce low-crystalline HAP with uniformly distributed nanoparticles [47–49].

In our study, the incorporation of Zn^{2+} ions into hydroxyapatite (HAP) was investigated. Zinc (Zn) is a critical trace element in humans, constituting approximately 3 g in the adult body. It serves both catalytic and structural roles in various biological processes, including metabolism, cell division, and gene transcription. Zinc deficiency is detrimental, particularly affecting the immune system [12]. Zinc is found as a trace element in bone. The introduction of Zn cations into the HAP structure is a popular area of research. The substitution of Zn^{2+} ions for Ca^{2+} results in a decrease in the lattice parameters a and c. This is due to the difference in the ionic radii of these cations (Zn^{2+} (0.074 nm) and Ca^{2+} (0.099 nm)). Scientific publications have reported that zinc stimulates bone formation by activating osteoblast proliferation and differentiation [50,51]. Zn-HAP also has antibacterial

properties against Gram-negative and Gram-positive bacteria. HAP doped with less than 1% zinc ions exhibits effective biological activity [12].

In previous studies, Zn-HAP coatings have been obtained by different methods, e.g., plasma spraying, sputtering, sol-gel method, magnetron sputtering. The Zn-HAP samples obtained by the different methods show a different distribution of zinc in the coating. For example, sputtering produces homogeneous Zn-HAP coatings, whereas magnetron sputtering produces Zn-HAP coatings with a higher concentration of zinc ions on the coating surface [12]. The dependence of the Zn-HAP biological response on the zinc content has been investigated in various experiments. Webster et al. have shown that even small amounts of Zn (from 1.3%) increase the osteoblast response [52]. In vitro adhesion and proliferation studies have shown that human osteoblast cells respond better to Zn-HAP layers compared to pure HAP coatings. Zn substitution was shown to affect the adhesion of HAP coatings on Ti substrates.

Another cation included in our research was Cu^{2+}. The introduction of Cu ions into the HAP structure also provides antibacterial properties to the HAP, which reduces the risk of inflammation after implantation. Additionally, our research examines the incorporation of Cu^{2+} ions into hydroxyapatite (HAP). Copper ions enhance protein absorption and osteogenic differentiation, and facilitate bone-like apatite formation at implant sites [53]. While Cu-based nanoparticles have catalytic applications due to copper's variable oxidation states (0, I, II, III) [54], the impact of Cu^{2+} substitution on HAP structure remains understudied. Cu has antibacterial properties, promotes angiogenesis, and has low cytotoxicity. Despite promising applications in orthopaedics, the literature shows that commercial success is still a long way off. This is not only due to the burden of the regulatory processes involved in bringing metal-doped materials to the health market, but also due to the difficulty in proving the effect of the element experimentally. Today's challenges are to combine in the same study all the characteristics related to the element: material studies (chemical composition, phase composition, formation, biomechanical aspects, brittleness, mechanical strength, and oxidation resistance) and biological aspects (cytotoxicity, bactericidal, osteogenic and angiogenic properties) [55]. Cu is a trace element essential for numerous physiological functions, including respiration, energy production, and tissue formation [56]. It is crucial for bone collagen maturation and osteoblast function [57,58]. In a 70 kg adult, approximately 100 mg of Cu is distributed primarily in the skeleton, muscles, liver, and brain [59]. While the maximum adult dose is 10 mg/day, deficiency can result in conditions like anaemia, leucopenia, and bone fragility [55]. Prado et al. demonstrated experimentally that after 48 h, MRSA, *Klebsiella pneumoniae*, and *Acinetobacter baumannii* did not adhere to Cu-containing samples, unlike stainless steel [60]. Another study investigated the incidence of infections over one year in an intensive care unit. Some patients were placed in wards with Cu-alloy surfaces and others in conventional wards. The proportion of patients who developed an infection with MRSA or VRE (vancomycin-resistant enterococcus) was compared between the two types of wards. In wards with Cu, 7.1% of patients developed nosocomial infection, compared with 12.3% in standard wards, indicating that Cu-alloy surfaces significantly reduced nosocomial infections [61]. Three main mechanisms are described in the literature: (a) membrane and cell wall damage due to direct interaction with microbial surfaces; (b) release of component divalent metal ions; (c) generation of reactive oxygen species (ROS), which are known to be toxic to bacteria.

In 2008, the EPA acknowledged copper's antimicrobial properties, leading to its incorporation in various biomedical materials, including calcium phosphate bioceramics [62,63]. Key studies have substantiated the antimicrobial efficacy of Cu-doped hydroxyapatite (HAP). For instance, Stanic et al. reported a 95% reduction in *Escherichia coli*, *S. aureus*, and *Candida albicans* [64], while Li et al. found less than a 1% survival rate of *E. coli* after 24 h [64]. In 2019, Bhattacharjee et al. confirmed the material's effectiveness against *E. coli* and *S. aureus* [65]. In 2015, Huang et al. synthesised Cu-doped HAP coatings on titanium. The coatings were found to have an antimicrobial effect of >75% against *E. coli* [66]. In a study by Kalaivani et al., copper-doped $CaSiO_3$ coatings were synthesised and evaluated

for their antibacterial properties against *E. coli* and *S. aureus*. The results showed that the pure powder did not exhibit antibacterial properties, but the antibacterial activity gradually increased with increasing Cu content in the doped coatings [23]. Ghosh et al. coated Cu-doped hydroxyapatite on titanium with varying Cu content and tested these samples against *E. coli* and *S. aureus*. Their results showed that the number of viable bacteria decreased as the Cu content of the coatings increased, while the antibacterial activity of the Cu-free hydroxyapatite was very low. After 8 h of cultivation, the antibacterial activity of *E. coli* on Cu-HAP was 78% and that of *S. aureus* was 83%. Wolf-Brandstetter et al. performed similar studies with titanium implants coated with Cu-HAP layers. After 2 h of cultivation with *E. coli*, the coatings with the highest Cu content showed a significantly lower number of viable bacteria and this effect was prolonged to 12 h. The results also showed a reduction in adherent bacteria on implant surfaces after 12 h [67]. Although Cu-based biomaterials are generally effective against bacteria, the efficacy is influenced by various parameters, such as bacterial type (Gram-positive or Gram-negative), testing methodologies, experimental conditions, and Cu content variation. The ion release rate in biological media also plays a role. Gram-positive bacteria, with their negatively charged and thick peptidoglycan membranes (20–80 nm), are more susceptible to Cu-induced apoptosis, whereas Gram-negative bacteria possess a thinner peptidoglycan layer (6–15 nm) and an outer membrane that can act as a diffusion barrier [22,68]. A paramount strength of this study resides in its innovative approach to the low-temperature synthesis of hydroxyapatite (HAP) coatings; thereby the adhesion to titanium substrate is better and formation of TiO_2 is avoided. The incorporation of copper and zinc ions as dopants not only adds complexity to the material but also offers a platform for the exploration of multifunctional properties. Significantly, the study takes the crucial step of evaluating the antibacterial efficacy of these doped coatings, filling a gap in current research on HAP-based biomaterials. Analytical methods used in the study provide a robust foundation for the reported findings. Nevertheless, the study is not devoid of limitations. A comprehensive analysis of the coatings' mechanical properties, aside from their antibacterial attributes, could provide a more holistic understanding of their potential applications [69–71]. Moreover, the study would benefit from a broader comparative framework that situates the findings in relation to existing methods and materials for HAP coatings.

5. Conclusions

A crystalline calcium hydroxyapatite (HAP) with a very high homogeneity and degree of particle size distribution was successfully synthesised from $CaCO_3$ coatings by a dissolution-precipitation method at low temperature of 80 °C in aqueous media. The low-temperature precipitation-dissolution method was successfully used for the synthesis of partially Cu^{2+} ion-substituted HAP. However, the formation of HAP coatings doped with Zn^{2+} ions by the above method did not proceed as smoothly as expected. The different synthesis methods tested resulted in the formation of $Zn(OH)(NO_3)(H_2O)$, $Zn_3(OH)_4(NO_3)_2$ on the surface of the coating, leaving unreacted calcium carbonate. Antibacterial property tests showed that no zones of inhibition were detected in pure HAP. In the Cu-HAP and Zn-HAP coating, after incubation for 24 h at 37 °C, zones of inhibition were detected in the presence of a colony of *B. subtilis* bacteria. However, no zones of inhibition were detected in the presence of *Escherichia coli*.

Author Contributions: Conceptualisation, I.G. and D.S.; methodology, A.K.; formal analysis, L.L., D.V. and J.K. resources, A.K.; writing—original draft preparation, A.K and L.L.; writing—review and editing, A.K.; visualisation, I.G.; supervision, A.K. All authors have read and agreed to the published version of the manuscript.

Funding: This research received no external funding.

Institutional Review Board Statement: Not applicable.

Informed Consent Statement: Not applicable.

Data Availability Statement: Data are contained within the article.

Conflicts of Interest: The authors declare no conflict of interest.

References

1. In, Y.; Amornkitbamrung, U.; Hong, M.H.; Shin, H. On the Crystallization of Hydroxyapatite under Hydrothermal Conditions: Role of Sebacic Acid as an Additive. *ACS Omega* **2020**, *5*, 27204–27210. [CrossRef]
2. Szewczyk, A.; Skwira, A.; Ginter, M.; Tajer, D.; Prokopowicz, M. Microwave-Assisted Fabrication of Mesoporous Silica-Calcium Phosphate Composites for Dental Application. *Polymers* **2020**, *13*, 53. [CrossRef] [PubMed]
3. Teotia, A.K.; Raina, D.B.; Singh, C.; Sinha, N.; Isaksson, H.; Tagil, M.; Lidgren, L.; Kumar, A. Nano-Hydroxyapatite Bone Substitute Functionalized with Bone Active Molecules for Enhanced Cranial Bone Regeneration. *ACS Appl. Mater. Interfaces* **2017**, *9*, 6816–6828. [CrossRef] [PubMed]
4. Tas, A.C. Synthesis of biomimetic Ca-hydroxyapatite powders at 37 degrees C in synthetic body fluids. *Biomaterials* **2000**, *21*, 1429–1438. [CrossRef] [PubMed]
5. Kumar, M.; Kumar, R.; Kumar, S. Coatings on orthopedic implants to overcome present problems and challenges: A focused review. *Mater. Today Proc.* **2021**, *45*, 5269–5276. [CrossRef]
6. Cheng, Y.; Zhao, G.; Liu, H. Histological evaluation of collagen-hydroxyapatite composite as osseous implants in the repair of mandibular defect. *Chin. J. Reparative Reconstr. Surg.* **1998**, *12*, 74–76.
7. Park, J.; Kim, B.J.; Hwang, J.Y.; Yoon, Y.W.; Cho, H.S.; Kim, D.H.; Lee, J.K.; Yoon, S.Y. In-Vitro Mechanical Performance Study of Biodegradable Polylactic Acid/Hydroxyapatite Nanocomposites for Fixation Medical Devices. *J. Nanosci. Nanotechnol.* **2018**, *18*, 837–841. [CrossRef] [PubMed]
8. Shi, P.; Liu, M.; Fan, F.; Yu, C.; Lu, W.; Du, M. Characterization of natural hydroxyapatite originated from fish bone and its biocompatibility with osteoblasts. *Mater. Sci. Eng. C Mater. Biol. Appl.* **2018**, *90*, 706–712. [CrossRef]
9. Eliaz, N.; Metoki, N. Calcium Phosphate Bioceramics: A Review of Their History, Structure, Properties, Coating Technologies and Biomedical Applications. *Materials* **2017**, *10*, 334. [CrossRef]
10. Yasukawa, A.; Gotoh, K.; Tanaka, H.; Kandori, K. Preparation and structure of calcium hydroxyapatite substituted with light rare earth ions. *Colloids Surf. A: Physicochem. Eng. Asp.* **2012**, *393*, 53–59. [CrossRef]
11. Lin, K.; Chang, J. Structure and properties of hydroxyapatite for biomedical applications. In *Hydroxyapatite (HAp) for Biomedical Applications*; Elsevier: Amsterdam, The Netherlands, 2015; pp. 3–19.
12. Arcos, D.; Vallet-Regi, M. Substituted hydroxyapatite coatings of bone implants. *J. Mater. Chem. B* **2020**, *8*, 1781–1800. [CrossRef] [PubMed]
13. Trinkunaite-Felsen, J. Investigation of Calcium Hydroxyapatite Synthesized Using Natural Precursors. Ph.D. Thesis, Vilnius University, Vilnius, Lithuania, 2014.
14. Ishikawa, K.; Kareiva, A. Sol–gel synthesis of calcium phosphate-based coatings—A review. *Chemija* **2020**, *31*, 25–41. [CrossRef]
15. Jonauske, V.; Stanionyte, S.; Chen, S.-W.; Zarkov, A.; Juskenas, R.; Selskis, A.; Matijosius, T.; Yang, T.C.; Ishikawa, K.; Ramanauskas, R. Characterization of sol-gel derived calcium hydroxyapatite coatings fabricated on patterned rough stainless steel surface. *Coatings* **2019**, *9*, 334. [CrossRef]
16. Shi, R.; Hayashi, K.; Bang, L.T.; Ishikawa, K. Effects of surface roughening and calcite coating of titanium on cell growth and differentiation. *J. Biomater. Appl.* **2020**, *34*, 917–927. [CrossRef] [PubMed]
17. Yanyan, S.; Guangxin, W.; Wuhui, L.; Yaming, W.; Hayakawa, S.; Osaka, A. Conversion of sub-μm calcium carbonate (calcite) particles to hollow hydroxyapatite agglomerates in K2HPO4 solutions. *Nanotechnol. Rev.* **2020**, *9*, 945–960. [CrossRef]
18. Harris, J.; Mey, I.; Hajir, M.; Mondeshki, M.; Wolf, S.E. Pseudomorphic transformation of amorphous calcium carbonate films follows spherulitic growth mechanisms and can give rise to crystal lattice tilting. *CrystEngComm* **2015**, *17*, 6831–6837. [CrossRef]
19. Gheisari, H.; Karamian, E.; Abdellahi, M. A novel hydroxyapatite—Hardystonite nanocomposite ceramic. *Ceram. Int.* **2015**, *41*, 5967–5975. [CrossRef]
20. Shanmugam, S.; Gopal, B. Copper substituted hydroxyapatite and fluorapatite: Synthesis, characterization and antimicrobial properties. *Ceram. Int.* **2014**, *40*, 15655–15662. [CrossRef]
21. Unabia, R.B.; Bonebeau, S.; Candidato Jr, R.T.; Jouin, J.; Noguera, O.; Pawłowski, L. Investigation on the structural and microstructural properties of copper-doped hydroxyapatite coatings deposited using solution precursor plasma spraying. *J. Eur. Ceram. Soc.* **2019**, *39*, 4255–4263. [CrossRef]
22. Bari, A.; Bloise, N.; Fiorilli, S.; Novajra, G.; Vallet-Regi, M.; Bruni, G.; Torres-Pardo, A.; Gonzalez-Calbet, J.M.; Visai, L.; Vitale-Brovarone, C. Copper-containing mesoporous bioactive glass nanoparticles as multifunctional agent for bone regeneration. *Acta Biomater.* **2017**, *55*, 493–504. [CrossRef]
23. Kalaivani, S.; Singh, R.K.; Ganesan, V.; Kannan, S. Effect of copper (Cu(2+)) inclusion on the bioactivity and antibacterial behavior of calcium silicate coatings on titanium metal. *J. Mater. Chem. B* **2014**, *2*, 846–858. [CrossRef]
24. Chandra, G.; Pandey, A. Biodegradable bone implants in orthopedic applications: A review. *Biocybern. Biomed. Eng.* **2020**, *40*, 596–610. [CrossRef]
25. León, B.; Jansen, J.A. *Thin Calcium Phosphate Coatings for Medical Implants*; Springer: Berlin/Heidelberg, Germany, 2009; Volume 309.

26. Prasad, K.; Bazaka, O.; Chua, M.; Rochford, M.; Fedrick, L.; Spoor, J.; Symes, R.; Tieppo, M.; Collins, C.; Cao, A.; et al. Metallic Biomaterials: Current Challenges and Opportunities. *Materials* **2017**, *10*, 884. [CrossRef]
27. Rieu, J.; Goeuriot, P. Ceramic composites for biomedical applications. *Clin. Mater.* **1993**, *12*, 211–217. [CrossRef]
28. Tang, X.; Thankappan, S.K.; Lee, P.; Fard, S.E.; Harmon, M.D.; Tran, K.; Yu, X. Polymeric biomaterials in tissue engineering and regenerative medicine. In *Natural and Synthetic Biomedical Polymers*; Elsevier: Amsterdam, The Netherlands, 2014; pp. 351–371.
29. De Long, W.G., Jr.; Einhorn, T.A.; Koval, K.; McKee, M.; Smith, W.; Sanders, R.; Watson, T. Bone grafts and bone graft substitutes in orthopaedic trauma surgery. *A critical analysis. J. Bone Jt. Surg. Am.* **2007**, *89*, 649–658. [CrossRef]
30. Fox, K.; Tran, P.A.; Tran, N. Recent advances in research applications of nanophase hydroxyapatite. *Chemphyschem* **2012**, *13*, 2495–2506. [CrossRef] [PubMed]
31. Siddiqui, H.A.; Pickering, K.L.; Mucalo, M.R. A Review on the Use of Hydroxyapatite-Carbonaceous Structure Composites in Bone Replacement Materials for Strengthening Purposes. *Materials* **2018**, *11*, 1813. [CrossRef] [PubMed]
32. Nasar, A. Hydroxyapatite and its coatings in dental implants. In *Applications of Nanocomposite Materials in Dentistry*; Elsevier: Amsterdam, The Netherlands, 2019; pp. 145–160.
33. Jeong, S.H.; Fan, Y.F.; Baek, J.U.; Song, J.; Choi, T.H.; Kim, S.W.; Kim, H.E. Long-lasting and bioactive hyaluronic acid-hydroxyapatite composite hydrogels for injectable dermal fillers: Physical properties and in vivo durability. *J. Biomater. Appl.* **2016**, *31*, 464–474. [CrossRef] [PubMed]
34. Sadat-Shojai, M.; Khorasani, M.T.; Dinpanah-Khoshdargi, E.; Jamshidi, A. Synthesis methods for nanosized hydroxyapatite with diverse structures. *Acta Biomater.* **2013**, *9*, 7591–7621. [CrossRef] [PubMed]
35. Ma, G. Three common preparation methods of hydroxyapatite. *Proc. IOP Conf. Ser. Mater. Sci. Eng.* **2019**, *688*, 033057. [CrossRef]
36. Pu'ad, N.M.; Haq, R.A.; Noh, H.M.; Abdullah, H.; Idris, M.; Lee, T. Synthesis method of hydroxyapatite: A review. *Mater. Today Proc.* **2020**, *29*, 233–239. [CrossRef]
37. Fihri, A.; Len, C.; Varma, R.S.; Solhy, A. Hydroxyapatite: A review of syntheses, structure and applications in heterogeneous catalysis. *Coord. Chem. Rev.* **2017**, *347*, 48–76. [CrossRef]
38. Kalita, S.J.; Verma, S. Nanocrystalline hydroxyapatite bioceramic using microwave radiation: Synthesis and characterization. *Mater. Sci. Eng. C Mater. Biol. Appl.* **2010**, *30*, 295–303. [CrossRef] [PubMed]
39. Lamkhao, S.; Phaya, M.; Jansakun, C.; Chandet, N.; Thongkorn, K.; Rujijanagul, G.; Bangrak, P.; Randorn, C. Synthesis of Hydroxyapatite with Antibacterial Properties Using a Microwave-Assisted Combustion Method. *Sci. Rep.* **2019**, *9*, 4015. [CrossRef] [PubMed]
40. Utara, S.; Klinkaewnarong, J. Effect of sonication time on the characteristics of nanophase hydroxyapatite crystals synthesised by the sol–gel technique. *Micro Nano Lett.* **2015**, *10*, 1–4. [CrossRef]
41. Akram, M.; Ahmed, R.; Shakir, I.; Ibrahim, W.A.W.; Hussain, R. Extracting hydroxyapatite and its precursors from natural resources. *J. Mater. Sci.* **2014**, *49*, 1461–1475. [CrossRef]
42. Sun, R.-X.; Lv, Y.; Niu, Y.-R.; Zhao, X.-H.; Cao, D.-S.; Tang, J.; Sun, X.-C.; Chen, K.-Z. Physicochemical and biological properties of bovine-derived porous hydroxyapatite/collagen composite and its hydroxyapatite powders. *Ceram. Int.* **2017**, *43*, 16792–16798. [CrossRef]
43. Googerdchian, F.; Moheb, A.; Emadi, R.; Asgari, M. Optimization of Pb(II) ions adsorption on nanohydroxyapatite adsorbents by applying Taguchi method. *J. Hazard. Mater.* **2018**, *349*, 186–194. [CrossRef] [PubMed]
44. Khoo, W.; Nor, F.; Ardhyananta, H.; Kurniawan, D. Preparation of natural hydroxyapatite from bovine femur bones using calcination at various temperatures. *Procedia Manuf.* **2015**, *2*, 196–201. [CrossRef]
45. Öksüz, K.E.; Kilinç, S.; Özer, A. Effect of calcination on microstructure development and properties of hydroxyapatite powders extracted from human and bovine bones. *Trans. Indian Ceram. Soc.* **2019**, *78*, 41–45. [CrossRef]
46. Varadavenkatesan, T.; Vinayagam, R.; Pai, S.; Kathirvel, B.; Pugazhendhi, A.; Selvaraj, R. Synthesis, biological and environmental applications of hydroxyapatite and its composites with organic and inorganic coatings. *Prog. Org. Coat.* **2021**, *151*, 106056. [CrossRef]
47. Gopi, D.; Kanimozhi, K.; Bhuvaneshwari, N.; Indira, J.; Kavitha, L. Novel banana peel pectin mediated green route for the synthesis of hydroxyapatite nanoparticles and their spectral characterization. *Spectrochim. Acta A Mol. Biomol. Spectrosc.* **2014**, *118*, 589–597. [CrossRef] [PubMed]
48. Gopi, D.; Kanimozhi, K.; Kavitha, L. Opuntia ficus indica peel derived pectin mediated hydroxyapatite nanoparticles: Synthesis, spectral characterization, biological and antimicrobial activities. *Spectrochim. Acta A Mol. Biomol. Spectrosc.* **2015**, *141*, 135–143. [CrossRef]
49. Begum, Y.; Deka, S. Green synthesis of pectin mediated hydroxyapatite nanoparticles from culinary banana bract and its characterization. *Acta Aliment.* **2017**, *46*, 428–438. [CrossRef]
50. Yamaguchi, M.; Oishi, H.; Suketa, Y. Stimulatory effect of zinc on bone formation in tissue culture. *Biochem. Pharmacol.* **1987**, *36*, 4007–4012. [CrossRef]
51. Yamaguchi, M. Role of zinc in bone formation and bone resorption. *J. Trace Elem. Exp. Med. Off. Publ. Int. Soc. Trace Elem. Res. Hum.* **1998**, *11*, 119–135. [CrossRef]
52. Webster, T.J.; Massa-Schlueter, E.A.; Smith, J.L.; Slamovich, E.B. Osteoblast response to hydroxyapatite doped with divalent and trivalent cations. *Biomaterials* **2004**, *25*, 2111–2121. [CrossRef] [PubMed]

53. Bulina, N.V.; Eremina, N.V.; Vinokurova, O.B.; Ishchenko, A.V.; Chaikina, M.V. Diffusion of Copper Ions in the Lattice of Substituted Hydroxyapatite during Heat Treatment. *Materials* **2022**, *15*, 5759. [CrossRef]
54. Othmani, M.; Bachoua, H.; Ghandour, Y.; Aissa, A.; Debbabi, M. Synthesis, characterization and catalytic properties of copper-substituted hydroxyapatite nanocrystals. *Mater. Res. Bull.* **2018**, *97*, 560–566. [CrossRef]
55. Jacobs, A.; Renaudin, G.; Forestier, C.; Nedelec, J.M.; Descamps, S. Biological properties of copper-doped biomaterials for orthopedic applications: A review of antibacterial, angiogenic and osteogenic aspects. *Acta Biomater.* **2020**, *117*, 21–39. [CrossRef]
56. Chellan, P.; Sadler, P.J. The elements of life and medicines. *Philos. Trans. A Math. Phys. Eng. Sci.* **2015**, *373*, 20140182. [CrossRef] [PubMed]
57. Opsahl, W.; Zeronian, H.; Ellison, M.; Lewis, D.; Rucker, R.B.; Riggins, R.S. Role of copper in collagen cross-linking and its influence on selected mechanical properties of chick bone and tendon. *J. Nutr.* **1982**, *112*, 708–716. [CrossRef] [PubMed]
58. Lowe, N.M.; Lowe, N.M.; Fraser, W.D.; Jackson, M.J. Is there a potential therapeutic value of copper and zinc for osteoporosis? *Proc. Nutr. Soc.* **2002**, *61*, 181–185. [CrossRef]
59. Ingle, A.P.; Paralikar, P.; Shende, S.; Gupta, I.; Biswas, J.K.; da Silva Martins, L.H.; Rai, M. Copper in medicine: Perspectives and toxicity. In *Biomedical Applications of Metals*; Springer: Berlin/Heidelberg, Germany, 2018; pp. 95–112.
60. Prado, J.V.; Esparza, M.M.; Vidal, A.R.; Duran, T.C. Adherence to copper and stainless steel metal coupons of common nosocomial bacterial strains. *Rev. Med. Chil.* **2013**, *141*, 291–297. [CrossRef]
61. Salgado, C.D.; Sepkowitz, K.A.; John, J.F.; Cantey, J.R.; Attaway, H.H.; Freeman, K.D.; Sharpe, P.A.; Michels, H.T.; Schmidt, M.G. Copper surfaces reduce the rate of healthcare-acquired infections in the intensive care unit. *Infect. Control Hosp. Epidemiol.* **2013**, *34*, 479–486. [CrossRef] [PubMed]
62. Prather, V. Copper, brass and bronze kill pathogens-including "superbug" MRSA-responsible for hospital- and community-acquired infections. *CDA Press Release* **2008**, *25*, 1.
63. Dorozhkin, S.V. Calcium orthophosphates. *J. Mater. Sci.* **2007**, *42*, 1061–1095. [CrossRef]
64. Stanić, V.; Dimitrijević, S.; Antić-Stanković, J.; Mitrić, M.; Jokić, B.; Plećaš, I.B.; Raičević, S. Synthesis, characterization and antimicrobial activity of copper and zinc-doped hydroxyapatite nanopowders. *Appl. Surf. Sci.* **2010**, *256*, 6083–6089. [CrossRef]
65. Bhattacharjee, A.; Fang, Y.; Hooper, T.J.N.; Kelly, N.L.; Gupta, D.; Balani, K.; Manna, I.; Baikie, T.; Bishop, P.T.; White, T.J.; et al. Crystal Chemistry and Antibacterial Properties of Cupriferous Hydroxyapatite. *Materials* **2019**, *12*, 1814. [CrossRef] [PubMed]
66. Huang, Y.; Zhang, X.; Zhao, R.; Mao, H.; Yan, Y.; Pang, X. Antibacterial efficacy, corrosion resistance, and cytotoxicity studies of copper-substituted carbonated hydroxyapatite coating on titanium substrate. *J. Mater. Sci.* **2015**, *50*, 1688–1700. [CrossRef]
67. Wolf-Brandstetter, C.; Beutner, R.; Hess, R.; Bierbaum, S.; Wagner, K.; Scharnweber, D.; Gbureck, U.; Moseke, C. Multifunctional calcium phosphate based coatings on titanium implants with integrated trace elements. *Biomed. Mater.* **2020**, *15*, 025006. [CrossRef] [PubMed]
68. Nan, L.; Liu, Y.; Lu, M.; Yang, K. Study on antibacterial mechanism of copper-bearing austenitic antibacterial stainless steel by atomic force microscopy. *J. Mater. Sci. Mater. Med.* **2008**, *19*, 3057–3062. [CrossRef] [PubMed]
69. Thakur, A.; Sharma, S.; Ganjoo, R.; Assad, H.; Kumar, A. Anti-Corrosive Potential of the Sustainable Corrosion Inhibitors Based on Biomass Waste: A Review on Preceding and Perspective Research. *J. Phys. Conf. Series* **2022**, *2267*, 012079. [CrossRef]
70. Hikku, G.S.; Arthi, C.; Jeen Robert, R.B.; Jeyasubramanian, K.; Murugesan, R. Calcium phosphate conversion technique: A versatile route to develop corrosion resistant hydroxyapatite coating over Mg/Mg alloys based implants. *J. Magnes. Alloys* **2022**, *10*, 1821–1845. [CrossRef]
71. Singh, J.; Singh Chatha, S.; Singh, H. Microstructural and in-vitro characteristics of functional calcium silicate topcoat on hydroxyapatite coating for bio-implant applications. *Prog. Biomater.* **2022**, *11*, 95–108. [CrossRef]